Neural network-assisted humanisation of COVID-19 hamster transcriptomic data reveals matching severity states in human disease

Vincent D. Friedrich,[a,b,p] Peter Pennitz,[c,p] Emanuel Wyler,[d] Julia M. Adler,[e] Dylan Postmus,[f,g,h] Kristina Müller,[a] Luiz Gustavo Teixeira Alves,[d] Julia Prigann,[f,g,i] Fabian Pott,[f,g] Daria Vladimirova,[e] Thomas Hoefler,[e] Cengiz Goekeri,[c,j] Markus Landthaler,[d,k] Christine Goffinet,[f,g,h] Antoine-Emmanuel Saliba,[l,m] Markus Scholz,[a,n] Martin Witzenrath,[c,o] Jakob Trimpert,[e] Holger Kirsten,[a,q,*] and Geraldine Nouailles[c,q,**]

[a]University of Leipzig, Institute for Medical Informatics, Statistics, and Epidemiology, Leipzig, Germany
[b]Center for Scalable Data Analytics and Artificial Intelligence (ScaDS.AI), Leipzig, Germany
[c]Charité – Universitätsmedizin Berlin, Corporate Member of Freie Universität Berlin and Humboldt-Universität zu Berlin, Department of Infectious Diseases, Respiratory Medicine and Critical Care, Berlin, Germany
[d]Max Delbrück Center for Molecular Medicine in the Helmholtz Association (MDC), Berlin Institute for Medical Systems Biology (BIMSB), Berlin, Germany
[e]Freie Universität Berlin, Institut für Virologie, Berlin, Germany
[f]Charité – Universitätsmedizin Berlin, Corporate Member of Freie Universität Berlin and Humboldt-Universität zu Berlin, Institute of Virology, Berlin, Germany
[g]Berlin Institute of Health at Charité – Universitätsmedizin Berlin, Berlin, Germany
[h]Liverpool School of Tropical Medicine, Department of Tropical Disease Biology, Liverpool, United Kingdom
[i]Gladstone Institutes, San Francisco, USA
[j]Cyprus International University, Faculty of Medicine, Nicosia, Cyprus
[k]Humboldt-Universität zu Berlin, Institut fuer Biologie, Berlin, Germany
[l]Faculty of Medicine, Institute of Molecular Infection Biology (IMIB), University of Würzburg, Würzburg, Germany
[m]Helmholtz Institute for RNA-based Infection Research (HIRI), Helmholtz Center for Infection Research (HZI), Würzburg, Germany
[n]University of Leipzig, Faculty of Mathematics and Computer Science, Leipzig, Germany
[o]German Center for Lung Research (DZL), Berlin, Germany

eBioMedicine
2024;108: 105312
Published Online 23 September 2024
https://doi.org/10.1016/j.ebiom.2024.105312

Summary

Background Translating findings from animal models to human disease is essential for dissecting disease mechanisms, developing and testing precise therapeutic strategies. The coronavirus disease 2019 (COVID-19) pandemic has highlighted this need, particularly for models showing disease severity-dependent immune responses.

Methods Single-cell transcriptomics (scRNAseq) is well poised to reveal similarities and differences between species at the molecular and cellular level with unprecedented resolution. However, computational methods enabling detailed matching are still scarce. Here, we provide a structured scRNAseq-based approach that we applied to scRNAseq from blood leukocytes originating from humans and hamsters affected with moderate or severe COVID-19.

Findings Integration of data from patients with COVID-19 with two hamster models that develop moderate (Syrian hamster, *Mesocricetus auratus*) or severe (Roborovski hamster, *Phodopus roborovskii*) disease revealed that most cellular states are shared across species. A neural network-based analysis using variational autoencoders quantified the overall transcriptomic similarity across species and severity levels, showing highest similarity between neutrophils of Roborovski hamsters and patients with severe COVID-19, while Syrian hamsters better matched patients with moderate disease, particularly in classical monocytes. We further used transcriptome-wide differential expression analysis to identify which disease stages and cell types display strongest transcriptional changes.

*Corresponding author. Institute for Medical Informatics, Statistics, and Epidemiology (IMISE), Haertelstraße 16-18, 04107, Leipzig, Germany.
**Corresponding author. Charité – Universitätsmedizin Berlin, Corporate Member of Freie Universität Berlin and Humboldt-Universität zu Berlin, Department of Infectious Diseases, Respiratory Medicine and Critical Care, Charitéplatz 1, 10117, Berlin, Germany.
E-mail addresses: holger.kirsten@imise.uni-leipzig.de (H. Kirsten), geraldine.nouailles@charite.de (G. Nouailles).
[p]Co-first authors.
[q]Co-last authors.

Interpretation Consistently, hamsters' response to COVID-19 was most similar to humans in monocytes and neutrophils. Disease-linked pathways found in all species specifically related to interferon response or inhibition of viral replication. Analysis of candidate genes and signatures supported the results. Our structured neural network-supported workflow could be applied to other diseases, allowing better identification of suitable animal models with similar pathomechanisms across species.

Funding This work was supported by German Federal Ministry of Education and Research, (BMBF) grant IDs: 01ZX1304B, 01ZX1604B, 01ZX1906A, 01ZX1906B, 01KI2124, 01IS18026B and German Research Foundation (DFG) grant IDs: 14933180, 431232613.

Keywords: COVID-19; Cross-species analysis; Disease state matching; Single-cell RNA-seq; Hamster model; Deep learning

Research in context

Evidence before this study

The translational gap between preclinical animal models and human patients impedes the transferability and interpretability of insights gained from animal experiments. In literature, structured cross-species analysis pipelines that leverage the power of deep learning algorithms while preserving biological interpretability are still scarce. Due to the large number of studies, animal models and data sets generated, COVID-19 is well suited for exploring the potential of this approach. We searched PubMed for human whole blood scRNAseq data sets covering different COVID-19 severity degrees to conduct a cross-species disease state matching with generated data from two hamster species.

Added value of this study

We established a neural network-based framework to match COVID-19 disease severity levels across humans and hamster species on a single-cell level, while also developing metrics for measuring interspecies similarity considering biological pathways and differential gene expression. We observed a synergistic relationship between AI-based and biologically informed analyses. Our results indicate that monocytes dominate the early pro-inflammatory response in moderate COVID-19 disease of human patients and infected Syrian hamsters, while extensive neutrophil influx is one key factor in severe to fatal disease courses in patients with severe COVID-19 and Roborovski hamsters. These findings are consistent with early pandemic observations gathered from human patient data.

Implications of all the available evidence

We have shown that the translational gap between preclinical animal models and human patients can be narrowed by integrating robust deep learning models in combination with biologically informed analyses. Cross-species comparisons of single-cell RNA sequencing data are well poised to reveal similarities and differences at molecular and cellular level, extending far beyond COVID-19 research. Specifically, the described methodology allows to determine universal immune mechanisms, enabling clinical and laboratory scientists working with animal models to identify both the specific opportunities and limitations of their models.

Introduction

Animal models are essential for understanding host–pathogen interactions[1] and for evaluating new therapies, as demonstrated by the rapid response to the recent severe acute respiratory syndrome coronavirus type 2 (SARS-CoV-2) caused pandemic, which was greatly aided by animal studies.[2–4] Nonetheless, the 'translational gap' from animal models to human disease often remains a major challenge.[5] One means to minimise this gap is to implement unbiased tools, i.e. tools not requiring explicit biological pathway knowledge, such as neural network-based models.

COVID-19 presents a suitable disease for conducting proof-of-concept studies. Multiple well-documented and publicly accessible single-cell transcriptomic (scRNASeq) datasets derived from blood of patients with COVID-19 are available.[6–10] Patients with COVID-19 exhibit a range of disease severities, which is measured using the world health organization's (WHO) ordinal scale for disease severity[11] (WOS). Various suitable COVID-19 animal models, such as non-human primates, ferrets, hamsters, and transgenic mice, typically addressing specific human disease stages, have been reported.[12–16] Hamster models are particularly suitable, as Syrian hamsters (*Mesocricetus auratus*) develop a moderate and Roborovski hamsters (*Phodopus roborovskii*) a severe disease course upon experimental infection.[17–19] Recent studies using advanced machine learning algorithms have demonstrated that unbiased analysis can e.g. successfully evaluate different vaccination strategies for COVID-19

prevention.[20] However comprehensive translational comparisons across species especially on the molecular level are still an unmet need.

For an unbiased and omics-based comparative analysis across species, individual species datasets first need to be successfully integrated. Multiple approaches exist, with different trade-offs between eliminating batch effects and preserving biological variance.[21] Integration of information across multiple experiments was demonstrated by the so-called Human Lung Cell Atlas (HLCA) core data set,[22] where a neural network-based method called scANVI[23] was used to integrate 14 datasets. Integration across species was demonstrated to be feasible, although among the most challenging tasks.[21,24]

Neural network-based models can also assist in comparing biological signals and patterns in high-dimensional scRNAseq data. Variational Autoencoders (VAEs) are especially valuable for this purpose.[25,26] VAE models can represent gene expression data (about 20,000 genes) in a low-dimensional space using as few as 10 dimensions, while also capturing the most significant input signals. Thus, VAEs have been utilised in scRNAseq data analyses to model sparse data,[27] integrate data,[28,29] generate data[29–31] and perform reference mapping.[32] The development of scGen by the lab of Theis and colleagues is a vital application of VAEs.[29] scGen has the capability to deduce data points for conditions not present in the data. It successfully predicted LPS responses across various animal species,[29] as well as protein abundance from mRNA in cases of Alzheimer's dementia,[33] and gene expression patterns in mice, humans, and cancer cell-lines following chemical perturbations.[34]

Here, we employ an scGen-based framework to match COVID-19 disease severity levels across humans and hamster species, while also developing a metric for measuring interspecies similarity on a cellular level. To complement this, we used differential expression analysis to compare up- and downregulation at whole genome, candidate-gene and pathway level, across different species and severities. Our study demonstrates how analysis of omics datasets across different species, utilising VAEs and other bioinformatics methods, can help to identify strengths and limitations of specific animal models and their relationships to human disease states.

Methods

Ethics statement and blood sampling for scRNAseq analysis

All experiments involving animals were approved by relevant institutional and governmental authorities (Freie Universität Berlin and Landesamt für Gesundheit und Soziales Berlin, Germany, permit number 0086/20) and adhered to the Federation of European Laboratory Animal Science Associations (FELASA) guidelines and recommendations for the care and use of laboratory animals, which is equivalent to American ARRIVE guidelines. Detailed description of virus stocks and cell processing can be found in Supplemental Methods. Briefly, 500 µL whole blood per animal was depleted of red blood cells by lysis, counted and processed for single-cell RNA sequencing using 3′-based 10x Genomics chemistry according to the manufacturer's instructions and as we previously published.[35] Sequencing was performed on a Novaseq 6000 device (Illumina) according to the manufacturer's instructions resulting in sample averages of 34,387 reads per cell and sequencing saturation of 73.1% (Table S1).

Animals and infection

In application of the 3R principle, no separate animals were sacrificed for the purpose of this study. Instead, we re-used data (Syrian hamsters[35]) and blood samples (Roborovski hamsters[36,37]) from animals studied in our previously published research. As part of these experiments, 10- to 12-week-old female and male Syrian hamsters (*M. auratus*; RjHan:AURA, Janvier Labs, Saint-Berthevin, France) and Roborovski hamsters (*P. roborovskii*, German pet store) were kept in individually ventilated cages (Tecniplast, Buguggiate, Italy) in a BSL-3 laboratory with free access to food and water. To reduce housing-related distress, animals were kept in cages equipped with environmental enrichment (Carfil, Oud-Turnhout, Belgium) such as various nesting materials, aspen brick, pressed hay balls and paper tunnels to meet their natural behaviour. Moreover, they were housed in groups of maximum 3 (Syrian hamsters) and 6 (Roborovski hamsters) animals per cage. For the duration of the infection experiments, the cage temperature and relative humidity were set between 22 and 24 °C and 40 and 55%, respectively. Before each experiment, the animals were allowed to acclimatise to the experimental conditions for at least 7 days.

As described in previous work,[38] Syrian and Roborovski hamsters were anaesthetised and intranasally infected using standardised procedures with 1×10^5 or 1×10^4 plaque-forming units (pfu) SARS-CoV-2 (variant B1, isolate BetaCoV/Germany)/BavPat1/2020). We performed clinical examination of all infected animals twice daily. Animals with a body weight loss of more than 15% for more than 48 h were euthanised according to the animal use protocol. In all other instances, naive hamsters (n = 3) and hamsters at 2, 3, 5 and 14 days after infection (n = 3 each) were randomly selected for sample collection. As described in our previous work,[36] euthanasia was carried out by cervical dislocation and exsanguination under anaesthesia. No statistical method was used to predetermine sample size. Instead, we selected a sample size of 3 animals per time point based on our previous experience with SARS-CoV-2 infection of Roborovski dwarf hamsters and Syrian hamsters. To

adhere to the 3R principle, we reduced the number of animals used in this study to the minimum that had been experimentally determined in our previous studies.[38–41] For ethical reasons, blinding of live animals was not possible because treatments had to be recorded on cage cards. No animals were excluded from the study. The hamster blood sampling schedule reflected the disease course of the hamster species: Roborovski hamsters experience a severe to fatal disease course, meeting humane endpoint criteria at 3 days post-infection (dpi), while Syrian hamsters undergo a transient, moderate disease course that allows for follow-up analyses of virus clearance and resolution of inflammation after high-dose infection. Thus, additional 5 dpi and 14 dpi time-points were sampled for Syrian hamsters. For human data, actual time-point of infection was unknown. Human data were grouped by WOS quantifying disease severity, and included patients with WOS3, WOS4, WOS5 and WOS7.

Data integration

Orthologue genes were defined based on Ensembl release 109–Feb 2023, for *P. roborovskii,* orthologue information from *M. auratus, Rattus_norvegicus, or Mus_musculus* was used as available (Figure S1, Table S2). The datasets of the three species (including cells marked as low quality) were integrated using anchor-based reversed PCA as implemented in the IntegrateLayers() function of the R-package Seurat. Cell clusters were identified again and visualised by embedding expression profiles in a Uniform Manifold Approximation and Projection (UMAP). For each cluster of cells, we identified the most likely cell type according to the originally reported cell label which was in line with reported marker genes. Cells with discordance between cluster and original label were removed (5.5%). Clusters from single species and integrated analyses with more than 50% cells not meeting cut-offs were removed if not explained by cell type (i.e. neutrophils and plasmablast cluster). Individual low-quality cells were also removed, in total 6.3% of all cells (Table S3).

VAE disease state matching

We applied variational autoencoders (VAEs) for jointly embedding high-dimensional hamster and human gene expression data into a low-dimensional latent space using the python package scGen[29] v2.0.0. Separate VAE models were trained for comparisons between humans and Syrian hamsters as well as between humans and Roborovski hamsters. Details on the VAE model and training hyperparameters are provided in Supplemental Methods. To account for diverse transcriptomic responses to infection across cell types, distinct VAE models were learned for each cell type. General interspecies differences in latent space were addressed by a species-shift-vector based exclusively on human controls (WOS0) and hamster controls (Day0). The control group-based species-shift-vector ensured controlling for interspecies difference while avoiding interference from infection response. To allow for cross-species disease state comparison, the species-shift-vector derived from the controls was applied to the latent embeddings of infectious hamster cells, a process we refer to as humanisation. The similarity between humanised-hamster disease states and human disease states was quantified via a diffusion pseudotime-based[42] distance metric d_2. Details can be found in Supplemental Methods.

Statistical analysis

R-package FDRtool 1.2.17 was used to estimate percentages of differential transcriptome in cells of infected vs. healthy subjects. Differential expression analysis of time points after infection compared to controls in hamsters, and WOS levels compared to controls in humans, were performed in the Limma-Voom[43] framework. We used standard-filtering for frequent genes, pseudo counts aggregated per biological replicate and included the calculation of confidence intervals (Table S4). Multiple testing of multiple genes was controlled by the false discovery rate according to Benjamini and Hochberg. To correlate fold-changes of genes expressed in the same direction in human patients and one hamster species, all genes significant at the level of FDR $\leq$ 20% in both species were used.

We followed standard procedures to ensure that the data met the assumptions of our statistical tests. As recommended, this involved constructing a DGEList object using the R package with appropriate library size normalisation using the calcNormFactors function. Only genes that met the suggested requirements were included in the pseudocount-based statistics by filtering them with the filterByExpr function from edgeR with default settings (min.count = 10, i.e. minimum count required for at least some samples; min.total.count = 15, i.e. minimum total count required; large.n = 10, i.e. number of samples per group that is considered "large"; min.prop = 0.7, i.e. minimum proportion of samples in the smallest group that express the gene). In addition, we inspected diagnostic plots for 'voom' after estimating observation and quality weights from the pseudo-bulk profiles, including a plot showing the mean-variance trend used to estimate the observation weights and another plot showing the per-sample quality weights, which appeared appropriate.

When comparing the top-10 differential regulated genes "corresponding direction" means either the same direction or, for timepoint 14 days post infection (dpi; i.e. recovered hamsters), the opposite direction between patients and hamsters. Pathway enrichment analyses were performed separately for each species and condition using gprofiler2 0.2.1. with the gene ontologies Biological Processes from Gene Ontology, Wikipathways,

Reactome, and KEGG. In this way, the foreground was defined as maximum 100 top-genes at FDR ≤ 20% ordered by absolute fold-change or–if this resulted in less than 30 genes–the top 30 genes ordered by *P*-value, excluding ribosomal and mitochondrial genes. The background were all genes considered in association analysis. When comparing overlapping pathways between species, we filtered for pathways being globally significantly enriched ($p_{adjusted} \leq 0.05$) and including at least 2 foreground-genes. No animals were excluded for any of the performed analysis.

Role of funders

The funders had no role in study design, data collection, data analysis, interpretation, or writing of the manuscript.

Results

We generated scRNAseq from blood of uninfected or infected Roborovski hamster (n = 3 per time point and condition) that received a low-dose (1×10^4 pfu) or a high-dose (1×10^5 pfu) of SARS-CoV-2 to compare with our previously published data from infected (1×10^5 pfu) and uninfected Syrian hamsters[35] and publicly available human data from patients with COVID-19 and controls[7] (Fig. 1a). All together the data encompass 28,357 cells in Syrian hamsters, 23,046 cells in Roborovski hamsters and 79,196 cells from humans.

Cellular recruitment in hamsters and humans

First, we combined blood transcriptomic data into a common embedding and applied a single unified gene nomenclature as described previously.[45] The merged dataset revealed species-related batch effects (Fig. 1b). To allow for application of a common cell type assignment, we resolved these by utilising the Reciprocal Principal Component Analysis (RPCA) data integration pipeline[46] to find a common embedding for the cells based on their cellular phenotypes rather than on experimental conditions (Fig. 1c). Application of Louvain-based clustering to integrated interspecies data identified several matching leukocyte populations (Fig. 1d, Figure S2). One previously described[7] subset of immature neutrophils, namely *FUT4*$^+$ pro-neutrophils (Immature Neutrophils 2), was exclusively observed in humans. In addition, while CD8$^+$-T-cells from hamsters clustered closer to CD4$^+$-T-cells, CD8$^+$-T-cells from patients with COVID-19 clustered closer to NK-cells (Fig. 1e), involving genes linked to cytotoxicity (*GZMA, NKG7, SLAMF7, CX3CR1, PRF1*), as well as transcription factors associated with T-cell effector/memory differentiation (*ZEB2, EOMES*) (Fig. 1f).

Examining the proportion of blood cell types over time after infection in hamster data, or with increasing disease severity in human data, revealed distinct patterns: Syrian hamsters experienced a sharp but transient increase in blood neutrophils at 2 days post-infection (dpi), resolving to basal levels by 3 dpi. In contrast, in both high- and low-dose infected Roborovski hamsters, neutrophils remained increased at 2 dpi and 3 dpi. In humans, a steady increase in the immature neutrophil fraction correlated with disease severity. The fraction of CD4$^+$-T-cells declined in patients with severe disease (WOS5, WOS7) compared to controls, which was consistent with both Roborovski hamster infection groups. By contrast, in patients with moderate disease course (WOS3, WOS4), CD4$^+$-T-cells increased. A reduction of non-classical monocytes, which is common in severe human disease,[6,7] was not observed in infected hamsters (Fig. 1g, Figure S3).

VAE-based neural network pipeline enables interspecies disease state matching of the transcriptome

To identify transcriptional similarities between humans and hamsters, we employed neural network techniques to match disease states across species. High-dimensional gene expression data was mapped to low-dimensional latent space through implementation of a variational autoencoder (VAE) model.[29] Latent embedding provides a denoised data representation, capturing only the most relevant input signals (Fig. 2a). For each hamster species and every cell type of interest, we trained separate VAE models for jointly embedding human and hamster data.

Fig. 2b illustrates the procedure to match disease states of human and Syrian hamster neutrophils using the example of finding the human severity grade corresponding best with Syrian hamster 2 dpi. In latent space, the species-shift-vector ($\delta_{species}$) is derived based on uninfected human and hamster controls via vector arithmetic (Supplemental Methods). Since only control groups were considered for computing $\delta_{species}$, it represents species differences, but not response to infection. The humanised representation of each hamster cell 2 dpi in latent space was then generated by applying $\delta_{species}$ to the cell's latent embedding and compared to the latent embeddings of human WOS5 and WOS7 cells by a similarity quantification of species disease states using graph-based diffusion pseudotime distance[42] incorporating 10 different root cells. For all root cells, humanised-hamster cells 2 dpi exhibited smaller mean diffusion pseudotime distance to human WOS5 cells (similarity score $d_2 = 0.92$) than to WOS7 cells ($d_2 = 0.083$) (Fig. 2b).

Species- and infection-shift-vectors in VAE latent space generalise to out-of-training samples

To evaluate the generalisability of the $\delta_{species}$ approach, we divided human and Syrian hamster neutrophil control groups into a training set and a test set (Fig. 3a, upper panel). $\delta_{species}$ was derived *de novo* solely from the VAE latent embeddings of the training set. Next, we

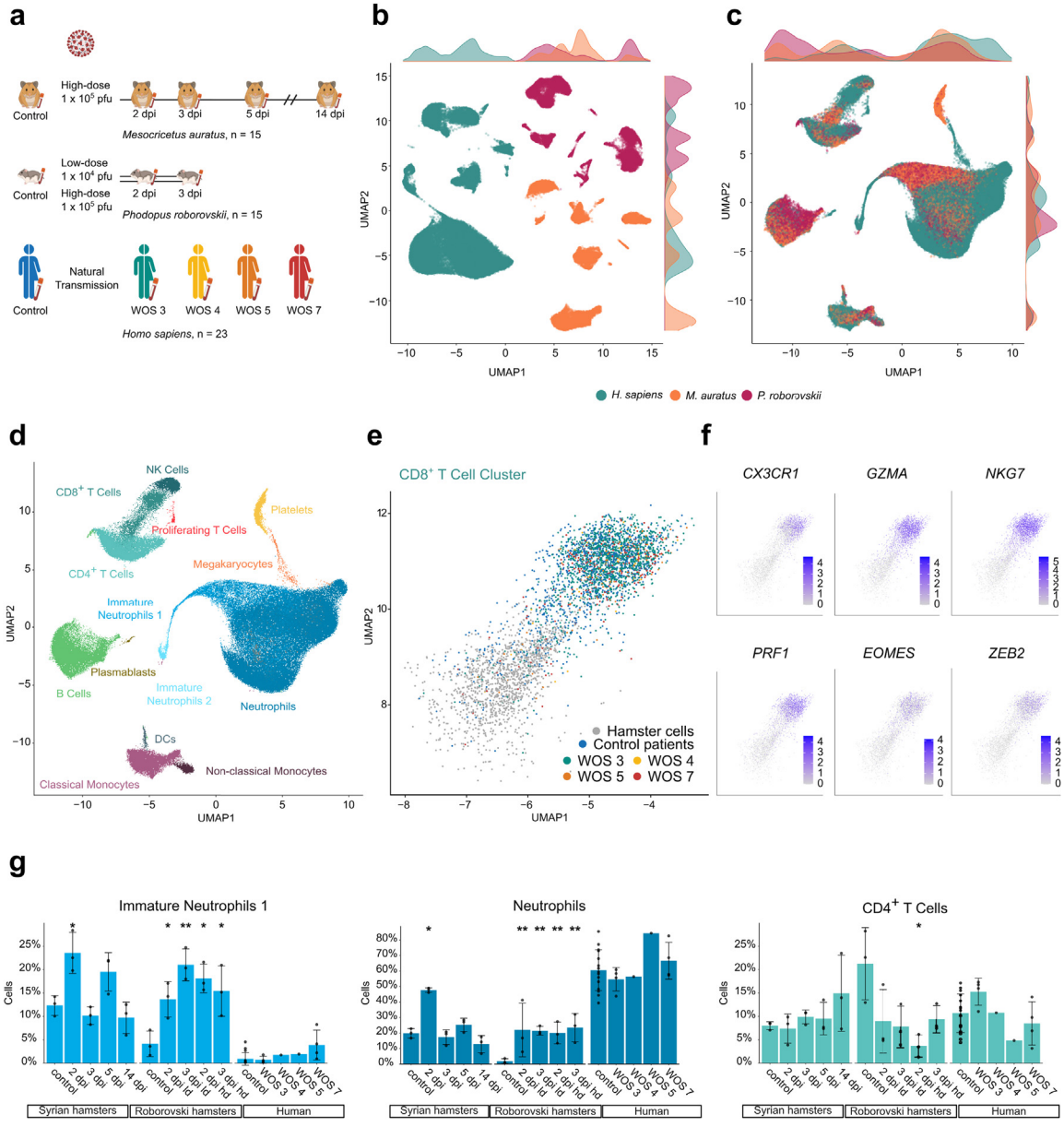

Fig. 1: **Cellular recruitment in hamsters and humans.** (**a**) Schematic overview of included datasets from humans and hamsters. (**b**) Uniform manifold approximation and projection (UMAP) plot indicating the original dataset of all cells merged in a common embedding before data integration including cell density per UMAP coordinate coloured according to species. (**c**) UMAP plot indicating the original dataset of all cells after performing data integration using Reciprocal Principal Component Analysis (RPCA) including cell density per UMAP coordinate coloured according to species. (**d**) UMAP plot of identified cell populations of all datasets. (**e**) UMAP Plot of $CD8^+$ T cell subset of human and hamster cells; colours indicate cells from different human severity levels. (**f**) UMAP plots of $CD8^+$ T cell subset indicating the expression of genes linked to cytotoxicity, and transcription factors associated with T cell effector/memory differentiation. (**g**) Frequencies of different populations in the two hamster species according to days post-infection and in humans according to the WHO ordinal scale for disease severity (WOS). To quantify significance of differential abundance of cell types, we applied a negative binomial generalised linear model as previously described.[44] * FDR ≤ 0.05, ** FDR ≤ 0.01. FDR: global false discovery rate. Data display means ± SD. n = 3 animals per time point for hamsters. Human Data: Cohort 2 from Schulte-Schrepping et al.[7] (Table S9).

applied the VAE encoder, $\delta_{species}$ and VAE decoder from the training set to the test set data, resulting in a decoded test set (Supplemental Methods). The application was considered successful, since the decoded test set of humanised-hamster cells displayed a stronger correlation with human data compared to the original decoded hamster data. Correlation was quantified using squared Spearman's rank correlation coefficient R^2 of all gene-

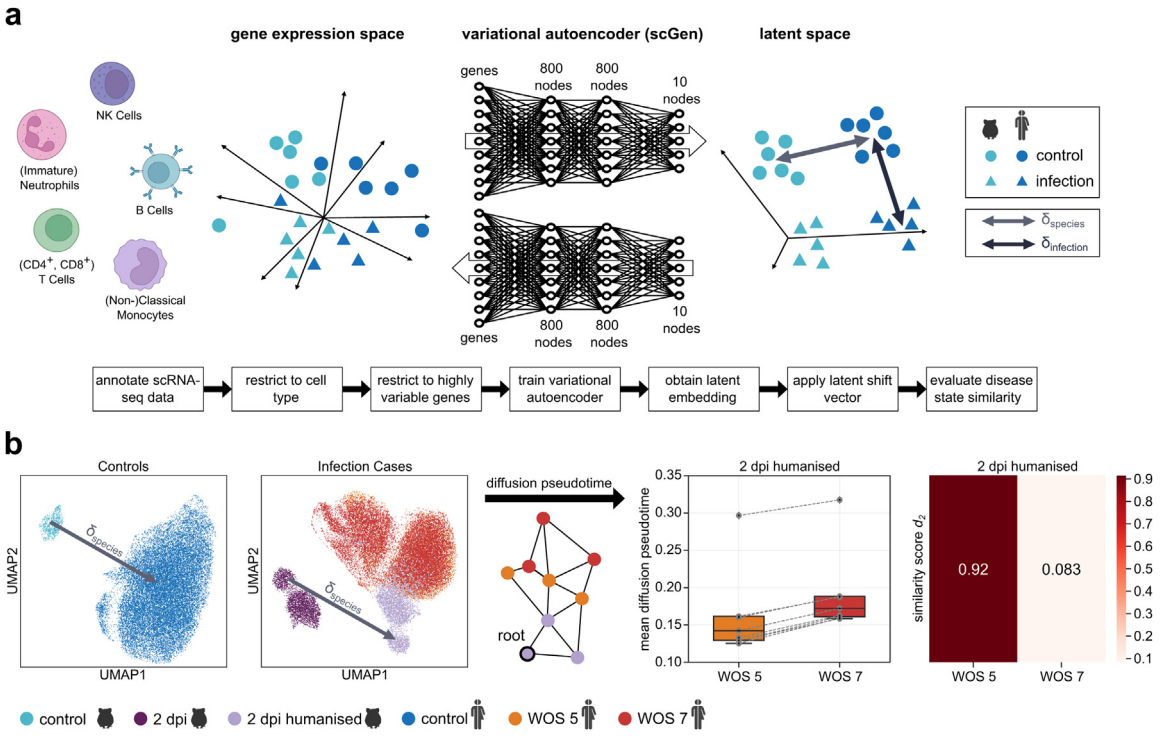

Fig. 2: **VAE neural network-based workflow enables interspecies disease state matching of the transcriptome.** (**a**) Schematic overview of the variational autoencoder (VAE) neural network-based pipeline for joint latent embeddings of high-dimensional hamster and human cell type-specific scRNAseq data. (**b**) Disease state matching in VAE latent space illustrated for Syrian hamster and human neutrophils with selected disease states. The species-shift-vector $\delta_{species}$ is derived from Syrian hamster and human controls (left panel, UMAP coordinates adapted) and applied to humanise the latent embedding of 2 dpi Syrian hamster cells (second left panel, UMAP coordinates adapted). To identify the best matching WOS grade, the mean diffusion pseudotime distances (graph-based, scheme middle panel) between the 2 dpi humanised Syrian hamster disease state and the human disease state WOS5 are calculated, as well as with the WOS7 state, respectively. For this we used 10 different root cells (second right panel), converted this information into a similarity score d_2 (right panel) and identified the best matching disease state. Boxplot specifications correspond to standard seaborn.boxplot v0.12. parameters.

wise calculated medians of species data with values ranging between 0 (no correlation) and 1 (perfect correlation). Decoded humanised-hamster achieved a higher R^2 score (0.97) compared to decoded original hamster (0.11) when tested against the gene expression of the human control group (Fig. 3a, lower panel) demonstrating generalisability of $\delta_{species}$ to out-of-training samples. Next, confirmation that humanisation works for both hamster species was achieved by repeating the training-test-split humanisation procedure with non-classical monocytes from Roborovski hamsters–again resulting in a higher R^2 score for decoded humanised-hamster (0.84) compared to decoded original hamster (0.27, Fig. 3b). Analogously, we tested the remaining cell types of both hamster species; humanisation worked properly at all occasions with best results for Syrian hamster (Figure S4).

We repeated the described training-test-split procedure to evaluate robustness of infection-shift-vectors $\delta_{infection}$ representing the mean direction of infection in latent space and enabling prediction of diseased states from a control cell. For the example of Syrian hamster neutrophils 2 dpi, the decoded predicted gene expression 2 dpi using control cells not used for training correlated more strongly with the decoded actual gene expression 2 dpi (R^2: 0.98) than with the corresponding control cell gene expression (R^2: 0.58) on the test set (Fig. 3c). Similar results were found for Roborovski hamster non-classical monocytes (R^2: 0.97 vs. R^2: 0.55, respectively) (Fig. 3d). This demonstrates that disease states can be addressed by an infection-shift-vector $\delta_{infection}$ in VAE latent space, which generalises to out-of-training samples.

VAE-driven mapping of hamster temporal disease states to patient severity levels

The VAE model pipeline was then used to map temporal disease states in hamsters to levels of disease severity in patients with COVID-19 across all datasets and cell types with sufficient cell counts. At all time points examined, resulting transcriptional states of most Syrian hamster cell types best matched patients with moderate disease based on similarity score d_2, particularly WOS3 and 4 (Fig. 4a, Figures S5a, b, S6a). However, for some cell types no clear assignment to a particular human severity

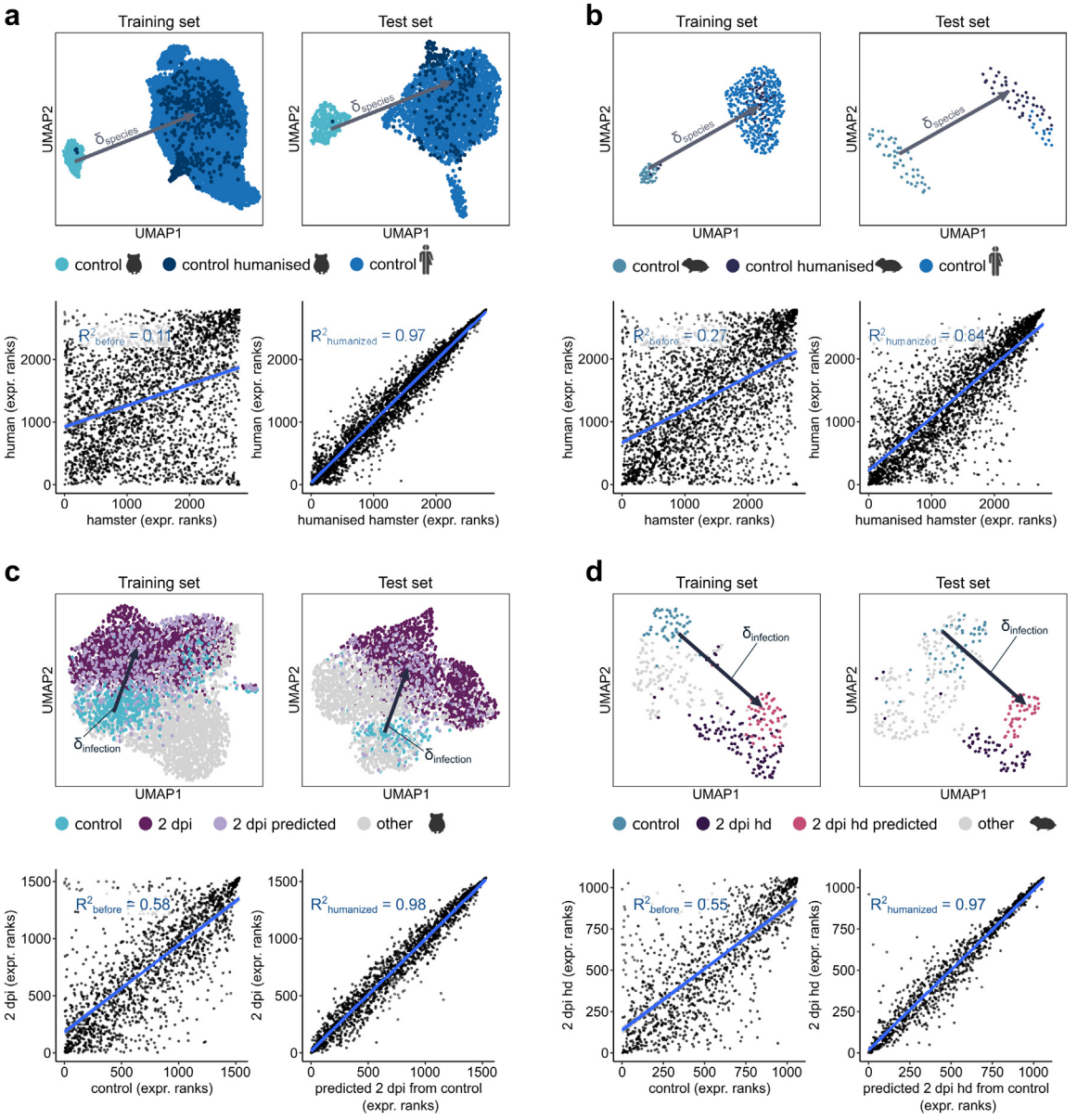

***Fig. 3*: Species- and infection-shift-vectors in VAE latent space generalise to out-of-training samples**. (**a**) Cross-species proof-of-principle for Syrian hamster and human neutrophil controls: The species-shift-vector $\delta_{species}$ in VAE latent space is derived solely from the training set (top left panel, UMAP coordinates adapted) and is applied to humanise the latent embeddings of hamster control cells of the test set (top right panel, UMAP coordinates adapted). Rank correlation scatter plots for decoded hamster and human gene expression (bottom left panel) as well as for decoded humanised hamster and human gene expression (bottom right panel) of the test set. (**b**) Analogous to (**a**) for Roborovski hamster and human non-classical monocyte controls. (**c**) Intra-species proof-of-principle for Syrian hamster neutrophils: The infection-shift-vector $\delta_{infection}$ is derived solely from the training set and points from control group towards the 2 dpi disease state in VAE latent space (top left panel, UMAP coordinates adapted). The 2 dpi disease state of control cells from the test set is predicted by applying the infection-shift-vector $\delta_{infection}$ from the training set in VAE latent space (top right panel, UMAP coordinates adapted). Rank correlation scatter plots for decoded control and 2 dpi gene expression (bottom left panel) as well as for decoded predicted 2 dpi and control gene expression (bottom right panel) on the test set. (**d**) Analogous to (**c**) for Roborovski hamster non-classical monocyte controls with predicted high-dose 2 dpi states of the control group. R^2: Spearman's rank correlation coefficient.

grade could be established. For example, transcriptomic profiles of Syrian hamster non-classical monocytes corresponded not only to that of patients with WOS3, as expected, but also resembled that of patients with WOS7. Among the Roborovski hamsters' blood leukocytes (Fig. 4b, Figures S5c, d, S6b), neutrophils,

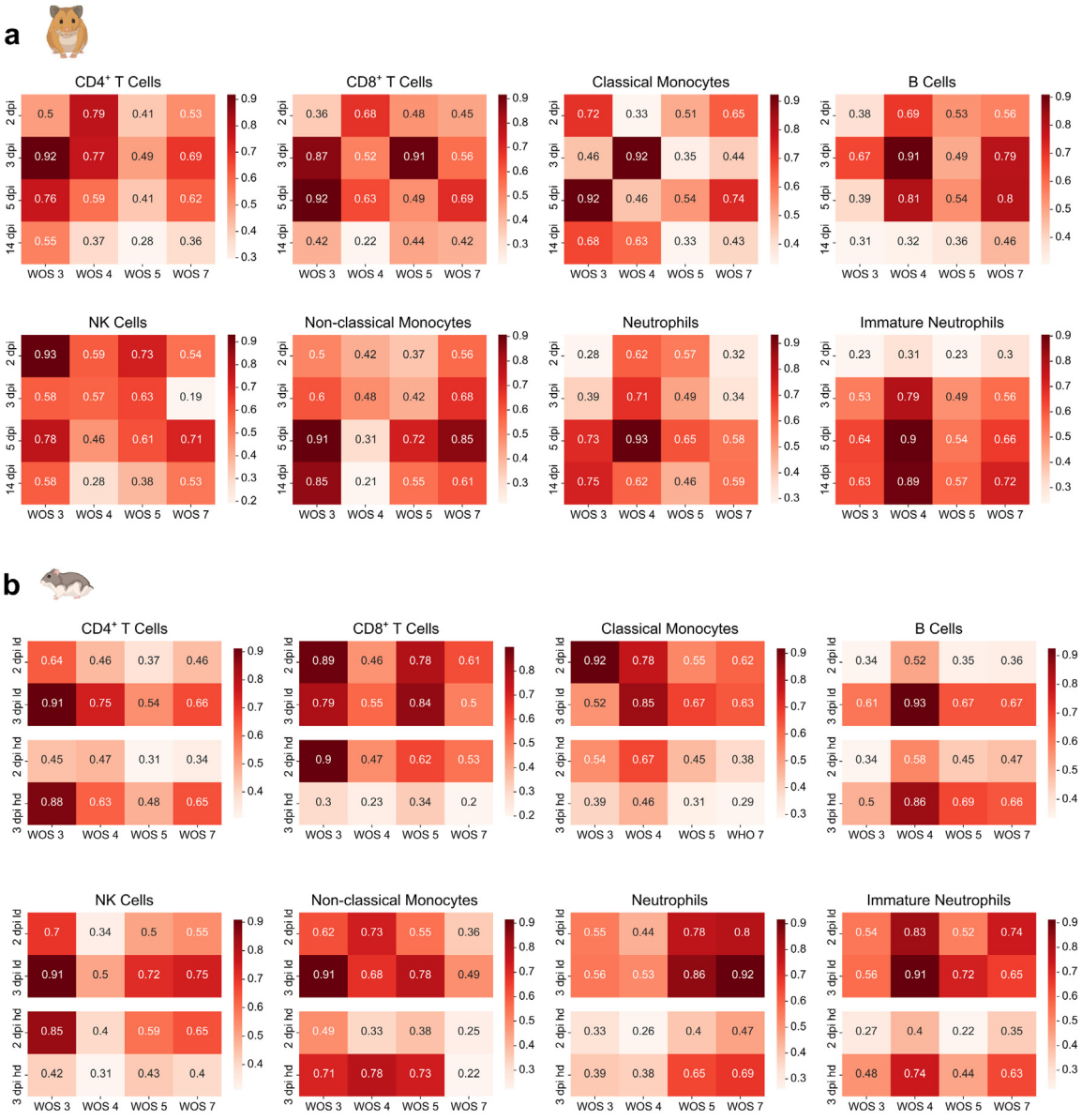

Fig. 4: **Neutrophils from Roborovski hamsters are the cell type that best matches that of patients with severe disease whereas Syrian hamster leukocytes are matched with moderate patient disease states.** Overall cell type-specific transcriptome similarity from VAE pipeline for each time point in hamsters to each severity score of human patients quantified as similarity score (d_2). Darker shades with higher values indicate higher similarity, corrected for species differences. (**a**) Similarity scores d_2 for pairs of human disease states (x-axis) and Syrian hamster disease states (y-axis). (**b**) Similarity scores d_2 for pairs of human disease states (x-axis) and Roborovski hamster disease states (y-axis). WOS: WHO ordinal scale; dpi: days post infection; ld: low dose; hd: high dose.

independently of infection dose, demonstrated highest similarity to patients with WOS7. Conversely, classical monocytes matched transcriptomic profiles of patients with moderate disease courses. Immature neutrophils of both hamster species matched patients with moderate but also showed similarity to patients with severe disease.

Differential gene expression correlation of human and hamster disease states

To examine which genes and pathways drive disease course similarities between patients with COVID-19 and hamster models, we conducted a differential gene expression (DGE) analysis of disease states compared to uninfected controls (Table S4).

Globally, Syrian and Roborovski hamsters showed the highest percentage of differentially regulated genes 2 dpi. In human patients, the highest percentage was observed in WOS7. To achieve the required minimum of two patients per group, patients with WOS4 and WOS5 were analysed together. However, this group still displayed the lowest statistical power, as evident by the notably lower fraction of differentially regulated genes (Fig. 5a, Table S5). We therefore focused on WOS3 and WOS7 and provide matching analyses for group WOS4 and WOS5 in the supplement (Figure S7). To identify similarities in antiviral responses, we probed if significant differential regulation in human patients and hamsters occurs in the same direction (Fig. 5b, Figure S7a). On single gene level, effect-sizes of significant genes showed little correlation between humans and hamsters. Yet, classical monocytes showed the highest number of similarly regulated genes between patients with WOS3 and 3 dpi and 5 dpi in Syrian hamsters, as well as with 2 dpi in high-dose Roborovski hamsters. In contrast, for patients with WOS7, the monocyte gene expression resembled all acute phase time points (i.e. ≤5 dpi) in both hamster species. Neutrophils showed strongest concordance of gene effect sizes between patients with WOS7 and 2 dpi as well as 3 dpi in Syrian and all Roborovski time points and doses, indicating increased activation of these cells in severe disease. In Syrian hamsters, neutrophils 5 dpi showed more concordance with WOS3. At 14 dpi, if at all, we only observed anti-correlated effect sizes of differentially regulated genes (e.g. $CD4^+$-T-cells) between humans and Syrian hamsters. This was likely due to the resolution of the Syrian hamster's infection by this point (Fig. 5b). Notably, despite small correlation of differentially expressed genes, overlapping differentially expressed pathways between species were highly specific for COVID-19, relating to interferon signalling and inhibition of viral replication (Fig. 5c, Figure S7b). They showed the most prominent co-enrichment in neutrophils of patients with WOS3 and Syrian as well as high-dose infected Roborovski hamsters. High co-enrichment was also observed in classical monocytes of patients with WOS3 and WOS7 as well as Syrian and high-dose infected Roborovski hamsters (Fig. 5c, Table S6). Cell–cell communication analysis (Supplemental Methods) supports the important role of neutrophils and monocytes in the antiviral response by revealing their high levels of communication. In general, a similarity between high and low communicating cell types, such as neutrophils and monocytes, is conserved across species. Syrian hamster disease states show higher variance, similar to humans (Fig. 6, Figure S8).

Common most highly differentially expressed genes in humans and hamsters after infection

Based on the analysis of correlated genes, we sought to identify the top 10 genes per cell type (ordered by absolute effect size at FDR 20%) regulated in matching directions in patients with COVID-19 and hamsters (Fig. 7, Figure S7c). Interferon-regulated genes, like *IFI27, IFIT2,* and *IFIT3*, were most abundant during the early phase of infection in hamsters and matched both patients with WOS3 and WOS7 across cell types. In neutrophils, all concordantly regulated top genes matched patients with severe disease progression. Most correlating neutrophil genes were expressed at 2 dpi in Roborovski hamsters. *LCN2,* a regulator of interferon-stimulated gene expression, prominently correlated between high- and low-dose infected Roborovski hamsters and patients with severe COVID-19. Further, *HP* upregulation and *CSF1R* downregulation correlated in the early disease neutrophils of hamster models and patients with severe disease. Interestingly, $CD4^+$-T-cells and NK-cells displayed a pattern of most top regulated genes correlating between patients with severe disease and Roborovski hamsters 2 dpi of high-dose infection (Fig. 7, Table S7).

COVID-19 mediators and gene expression patterns amongst relevant cell types

To further investigate which specific genes contribute to severe or moderate disease courses, we analysed genes described to associated with inflammation[35,41] (Fig. 8a, Figure S9a, b, Table S8). Several of these genes, such as interferon-stimulated genes (*IRF7, IFIT3, ISG15, ISG20*), chemokines (*CXCL10, CXCL11*) and pro-inflammatory mediators (*TNFSF10, NLRC5*) showed the highest expression levels in blood leukocytes of high-dose infected Roborovski hamsters. Low-dose infected Roborovski hamsters deteriorated less rapidly with fewer inflammatory genes expressed by classical monocytes. In human patients with COVID-19, the inflammatory response appeared more monocyte-dependent in moderate cases and neutrophil-dependent in severe cases. Interestingly, *S100A8, S100A9,* and *CD177* were not upregulated in hamsters, but were found to be upregulated in patients with WOS7 and associate with severe COVID-19[10,49] (Fig. 8a).

Finally, we analysed a "severe inflammatory" gene signature in neutrophils linked to severe disease in humans[50] (Table S7). This signature measures expression of 201 immune-related genes and was found in a subset of neutrophils of patients with WOS5 and WOS7 COVID-19. In Syrian hamsters, the gene scores in innate immune cells were low, whereas in Roborovski hamsters they were high, particularly in neutrophils of the high-dose infection group. Notably, this gene signature was not exclusively present in neutrophils, yet its severity-dependence was most prominent in neutrophils (Fig. 8b).

While this demonstrates an inflammatory response of Roborovski hamster neutrophils similar to patients with severe disease, a notable difference was that the gene set was found uniformly expressed in hamster

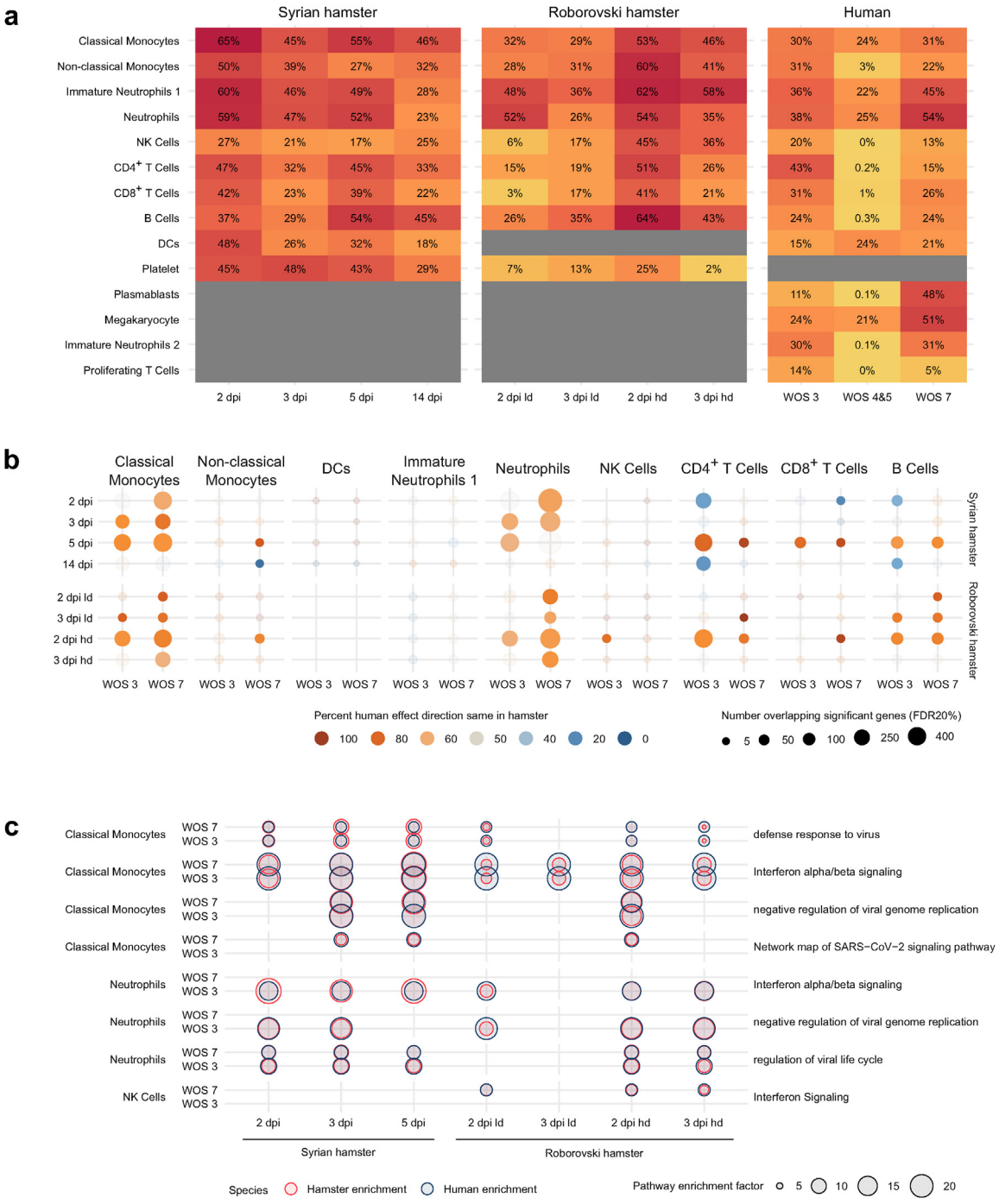

Fig. 5: **Differential gene expression correlation of human and hamster disease states.** (**a**) Percentage of genes significantly up- or downregulated in humans or hamster species compared to controls. (**b**) Dotplot indicating significantly regulated genes regulated in the same direction in humans and hamsters. Shown in bright colours are conditions where significantly more (orange) or less (blue) than 50% of the overlapping genes were regulated in the same direction. (**c**) Dotplot of pathways enriched in differentially expressed genes that are present in human and hamster species. Here we focus on specific pathways, i.e. pathways not including more than 220 genes and not being redundant regarding included genes (see Table S5 for all pathways present in both human and hamsters). Differential expression analyses were performed in the Limma-Voom[43] framework. Multiple testing adjustments were applied using the false discovery rate according to Benjamini and Hochberg. To correlate fold-changes, all genes significant at false discovery rate (FDR) ≤ 20% in both species were used. Pathway enrichment analyses for globally significant pathways (*P* corrected ≤ 0.05) were performed using gprofiler2. Pathway enrichment factor is the ratio between observed and expected proportion of significant genes in each pathway.

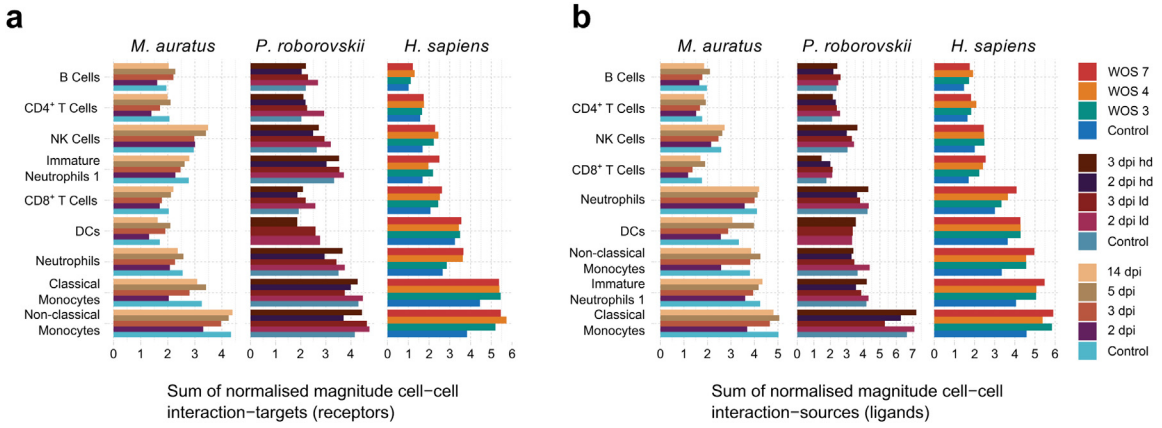

Fig. 6: **Cell–cell communication.** Shown is the sum of interaction magnitudes normalised by the number of ligands and receptors available to each cell type when acting as either target (**a**) or source (**b**), respectively. Cell–cell communication analyses were performed within the LIANA[47,48] framework.

neutrophils, but only in a specific subset of patients with severe disease (Figure S10a). Expression was high in the dense neutrophil-clusters "2" and "3" of patients with severe disease, but low in the remaining neutrophil-clusters (Figure S10a, b). Differential expression analysis on clusters 2 and 3 compared to the other neutrophil clusters in patients with severe COVID-19 further revealed elevated expression of inflammation-associated genes (Figure S10c, d). Notably, most of these genes were not included in the "severe inflammatory" signature and were yet highly expressed in "severe inflammatory" neutrophils (Figure S10e). In particular, genes associated with interferon response and TNFR signalling were highly expressed (Figure S10c, d). This suggests that the highly inflammatory response triggered by COVID-19 in human neutrophils is limited to a subset of these cells. Intriguingly, in Roborovski hamsters, the expression of the severe inflammatory signature was not restricted to a specific neutrophil subset.

VAE feature importance analysis

We applied explainable AI techniques to identify the top contributing genes to the VAE models used for cross-species disease state matching (Figures S11, S12). The top 141 contributing genes partially overlapped with differentially expressed genes, with only 5 not observed at FDR $\leq$ 5% (*SAMD3, FCER1A, SERPINB2, PTGDS,* and *FCGR2A*). These five are less than expected by chance ($p_{\text{Fisher's Exact}}$ < 2.2e-16) and all have relevance as immunity and inflammation mediators. Comparing the correlation between VAE gene importance and differential expression significance revealed frequent correlations, especially in neutrophils and monocytes. Pathway analysis of the top VAE genes consistently identified immune-related pathways, including interferon and antiviral responses, consistent with classical approaches from differential expression analysis (Fig. 4).

Discussion

Our study employs a machine learning-based approach[29] to bridge the persistent translational divide between preclinical animal models and clinical research in humans.[51] By integrating VAE neural network-based generative models, differential gene expression, and pathway analysis, we achieved a thorough comparison of disease responses at a single-cell level across different species. Our VAE-based disease-state-matching pipeline demonstrates the feasibility of inferring humanised versions of hamster cells, addressing interspecies differences directly in the VAE latent space and extending existing cross-species integration strategies.[52]

Our VAE-based analysis corroborates that the Syrian hamster model closely resembles the response of human patients with moderate COVID-19 across all relevant blood cell types. Differential expression analysis confirmed this in specific, but highly relevant cell types: For example, the interferon-related gene expression peaking 5 dpi in Syrian hamster classical monocytes resembles the immune response observed in immunocompetent patients,[53] while hamster neutrophils during early infection times match patients with WOS4 with modest inflammatory response gene expression patterns. In sum, our approach further supports that SARS-CoV-2-infected Syrian hamsters are a valid model for studying innate and adaptive immunity in moderate COVID-19, in congruence with their proven effectiveness for testing vaccination,[41] immune modulatory therapy,[54] and antiviral therapeutic strategies.[55,56]

While Roborovski hamsters infected with high-dose SARS-CoV-2 have been utilised as a model for severe COVID-19 disease due to their high susceptibility,[18,57] our bioinformatics workflow shows some limitations: neutrophils are the only immune cell type in this model that reflects severe clinical disease in humans. Moreover, the rapid and fatal disease progression in

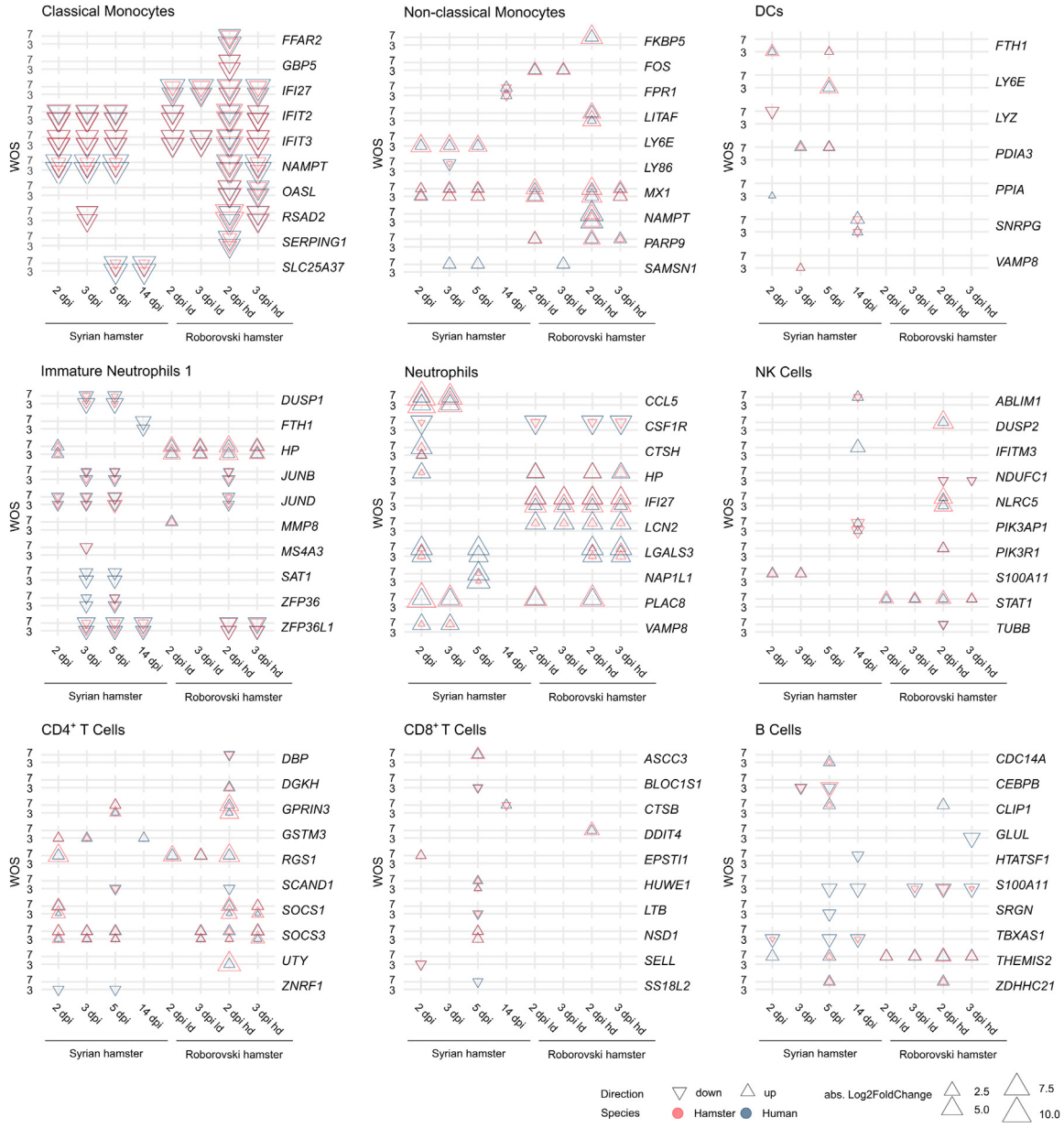

***Fig. 7:* Most common differentially expressed genes in humans and hamsters after infection.** Dotplot displaying the top 10 genes for each cell type (ordered by absolute effect size at FDR 20%) that are regulated in concordant direction (abs. Log2FoldChange) in humans and hamsters. Larger symbols correspond to larger effect sizes, direction of the triangles to up- or downregulation and colour to species. All common significantly expressed genes with corresponding fold-changes are reported in Table S6. Differential expression analyses were performed in the Limma-Voom[43] framework. Multiple testing adjustments were applied using the false discovery rate (FDR) according to Benjamini and Hochberg.

Roborovski hamsters precludes the study of adaptive immunity during severe disease, as animals reach humane endpoints before cells like exhausted T-cells[6] or pathologic CD16^{+} T-cells[58] can develop. Besides, human patients with severe COVID-19 also exhibit increased inflammatory responses by innate immune cells other than neutrophils, which Roborovski hamsters fail to represent well, e.g. dysfunctional Eomes^{hi}Tbet^{lo} NK-cells.[59] The same is true for the observed shift of inflammatory classical monocytes to "immunoparalysis" in severe COVID-19.[6] Multiple models may thus be required to simulate different aspects of severe human COVID-19, especially given the numerous risk factors influencing disease progression.[60,61] Hence, systematic

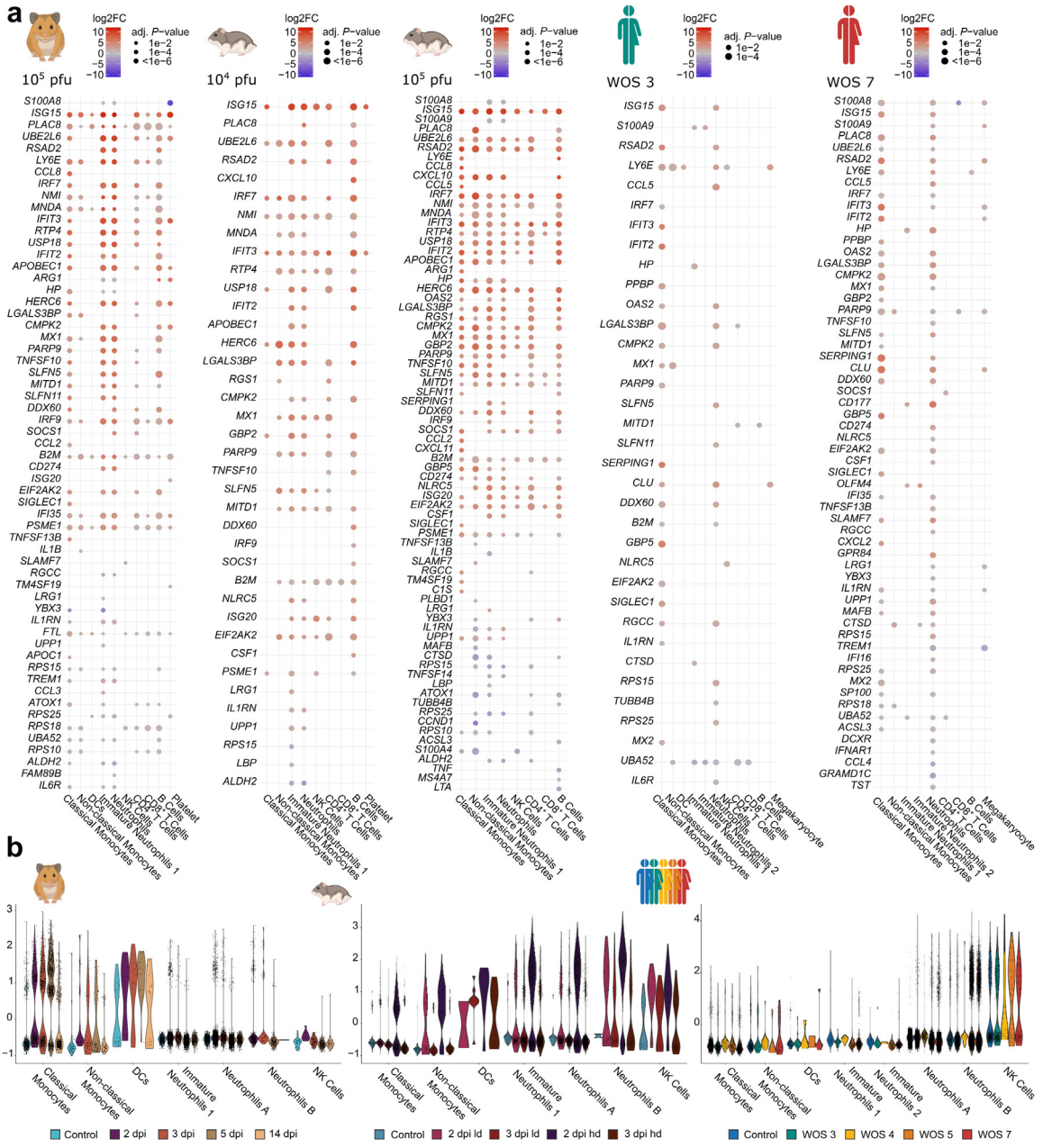

***Fig. 8*: COVID-19 mediators and gene expression patterns amongst relevant cell types.** (**a**) Dotplots displaying significantly up- or downregulated genes linked to inflammation in human patients by WOS severity level compared to controls or in hamster species 2 dpi compared to controls. (**b**) Violin plots displaying expression of the previously described "severe inflammatory" gene set[50] amongst different innate immune cell types in humans or hamster species. Differential expression analysis were performed in the Limma-Voom[43] framework. Log2FC: log2FoldChange, dpi: days post infection, adj. *P*-value: adjusted *P*-values were calculated according to Benjamini and Hochberg.

approaches as proposed here might be a helpful tool also in other diseases to identify which processes in specific animal-cell types reflect the human states.

The neutrophil bias observed in Roborovski hamsters infected with SARS-CoV-2 is consistent across different infection doses, indicating a predisposition which was likewise observed in their pulmonary COVID-19 immune response.[37] This bias does not align with the diverse cellular inflammatory responses seen in humans with severe COVID-19 and some key genes associated with poor outcome in patients, namely the alarmins *S100A8*/*S100A9* encoding for calprotectin[10]

and the neutrophil activation marker *CD177*,[49] were not prominently expressed in hamster neutrophils. Consequently, the utility of the Roborovski hamster as a severe disease model for translating mechanisms of therapeutic immune modulators remains limited to subsets of inflammatory neutrophils.[62]

Our VAE neural network-based approach provides an unbiased, rapid method for exploring scRNAseq data across species by providing a global similarity score without requiring ground truth labels, which may be difficult to obtain. In contrast, other COVID-19 machine learning studies in animals have required supervised techniques, e.g. for assessing virulence,[63] predicting infection,[64] and identifying essential genes for vaccination status classification.[20] For the latter, the reported top identified features (*DDX5*, *DEF6*, *EEF1A1*, *IFIT3*, *PFN1*, *RPS23*, *RPSA*, *TPT1*, *UBA52*) also showed an above-average importance in our VAE, indicating agreement in content between approaches.

By learning molecular differences between species, our VAE model can generate humanised molecular profiles derived from animal models. For example, in future applications, it could be trained to predict whether subgroups of patients are likely to be responders or non-responders to different doses or different drugs used in the animal model. It could also predict the molecular effects of untested treatment combinations in animal models, potentially reducing the number of subjects required for future experiments.

However, challenges arise in the selection of hyperparameters and the careful handling of orthologues. The performance of our VAE model depends on the quality and quantity of the underlying data. The lack of direct interpretability in the VAE latent space can be mitigated by evaluating the importance of each gene for the latent space, as shown here, or by modifying the VAE architecture to consider linear decoders.[65]

Importantly, comparison with results from classical analyses such as differential gene expression, cell–cell communication, and pathway importance provides another level of validation and molecular insights across species. For our model, we observed consistency, e.g. in the inclusion of immune and inflammatory pathways, or in the observed correlation between VAE significance and differential expression significance, with differences likely also reflecting the ability of VAE to capture both, interspecies differences and infection responses. Important VAE genes not observed among the top genes in classical analyses were meaningful in the context of infection. This suggests that the VAE approach complements traditional approaches in extracting key transcriptional features related to COVID-19 severity from the hamster models.

In conclusion, the combination of the global transcriptomic view provided by the VAE model, along with differential gene expression and pathway enrichment analysis, helps to narrow the 'translational gap' by providing a nuanced understanding of disease responses across species at the single cell level. It supports the identification of meaningful animal models that recapitulate human molecular dynamics for the development and testing of therapeutic interventions.

Limitations of the study

While offering valuable insights, our study has limitations. Sole reliance on blood data restricts organ-specific insights, e.g. on lungs as primary sites of infection or secondary lymphoid organs as sites of adaptive immune cell priming. Nonetheless, our focus on blood cells overcomes the problem that lung tissue is only available post-mortem from fatal cases, and oropharyngeal swabs as well as bronchoalveolar lavages, provide an incomplete picture of pulmonary cell types.[66,67] A further limitation involves the sample sizes of the analysed datasets which do not allow for subgroup analysis, for example regarding ethnic and sex-related patterns in response to COVID-19. To address the shortcoming of putative species-specific differences in cell activation pattern, sequencing-based lineage-tracing methods[68] could potentially help to identify common developmental pathways and to validate cross-species disease-specific cellular activation patterns on a computational level.

Contributors

Conceptualisation: VDF, PP, HK, GN; Methodology: VDF, PP, AES, EW, JT, HK, GN; Investigation: VDF, PP, EW, JMA, DP, KM, LGTA, JP, FP, DV, TH, CG, ML, CG, AES, MS, MW, JT, HK, GN; Formal analysis: VDF, PP, HK, GN; Visualisation: VDF, PP, HK, GN; Project administration: JT, HK, GN; Supervision: MS, MW, JT, HK, GN; Writing—original draft: VDF, PP, HK, GN. VDF, PP, HK verified the underlying data. All authors read and approved the final version of the manuscript.

Data sharing statement

Publicly available datasets that were used in this manuscript can be found at GEO: "GSE162208" (Syrian hamsters) and EGA: "EGAS00001004571" (humans). Datasets for Roborovski hamsters and processed data are available via GEO: "GSE253845" and Zenodo: https://zenodo.org/records/10580154. The code used for data analysis is available at github.com, https://github.com/GenStatLeipzig/Neural-Networks-Assisted-Humanization-of-COVID-19-Hamster-scRNASeq-data.

Declaration of interests

MS received funding from Pfizer Inc. for a project related to pneumococcal vaccination. MS receives funding from Owkin for a project not related to this research. MW reports grants and personal fees from Biotest, grants and personal fees from Pantherna, grants and personal fees from Vaxxilon, personal fees from Aptarion, personal fees from Astra Zeneca, personal fees from Chiesi, personal fees from Insmed, personal fees from Gilead, outside the submitted work. GN reports grants from Biotest AG outside the submitted work. Unrelated to this work, Freie Universität Berlin has filed a patent application (PCT/EP2022/051215) for SARS-CoV-2 vaccines. JT is named as inventor on this application and receives remuneration in accordance with German law ("*Gesetz über Arbeitnehmererfindungen*"). Freie Universität Berlin is collaborating with RocketVax Inc. for further development of SARS-CoV-2 vaccines and receives funding for research. The other authors declare no competing interest.

Acknowledgements

The authors thank Jeannine Wilde, Madlen Sohn, and Tatiana Borodina (MDC Scientific Genomics Platforms) for sequencing.

This work was supported by a Federal Ministry of Education and Research of Germany (BMBF) grant to MS, MW, HK and GN, grant number e:Med CAPSyS (01ZX1304B, 01ZX1604B) and e:Med SYMPATH (01ZX1906A, 01ZX1906B); MW and GN were supported by the BMBF in the framework of MAPVAP (01KI2124). MW received funding from the German Research Foundation (DFG; project ID 114933180—SFB-TR84, sub-projects C06 and C09 and project ID 431232613—SFB-1449, sub-project B02). JT received funding from the DFG (project ID 114933180—SFB-TR84, sub-project Z01b). VDF and HK were funded by the BMBF (01IS18026B) and by Sächsische Staatsministerium für Wissenschaft, Kultur und Tourismus (SMWK) in the program Center of Excellence for AI-research, Center for Scalable Data Analytics and Artificial Intelligence, Dresden/Leipzig, project identification number: ScaDS.AI. AES thanks CompLS BMBF funding HOPARL. Schemes as well as Hamster and human icons were created using BioRender.com. During the preparation of this work the authors used ChatGPT/OpenAI, Claude.ai/Anthropic and DeepL/DeepL SE in order to improve English language and grammar, as well as German to English translations. After using these tools, the authors reviewed and edited the content as needed and take full responsibility for the content of the publication.

Appendix A. Supplementary data

Supplementary data related to this article can be found at https://doi.org/10.1016/j.ebiom.2024.105312.

References

1 Dinnon KH 3rd, Leist SR, Okuda K, et al. SARS-CoV-2 infection produces chronic pulmonary epithelial and immune cell dysfunction with fibrosis in mice. *Sci Transl Med*. 2022;14(664):eabo5070.
2 Leenaars CHC, Kouwenaar C, Stafleu FR, et al. Animal to human translation: a systematic scoping review of reported concordance rates. *J Transl Med*. 2019;17(1):223.
3 Vogel AB, Kanevsky I, Che Y, et al. BNT162b vaccines protect rhesus macaques from SARS-CoV-2. *Nature*. 2021;592(7853):283–289.
4 Corbett KS, Flynn B, Foulds KE, et al. Evaluation of the mRNA-1273 vaccine against SARS-CoV-2 in nonhuman primates. *N Engl J Med*. 2020;383(16):1544–1555.
5 Ferreira GS, Veening-Griffioen DH, Boon WPC, Moors EHM, van Meer PJK. Levelling the translational gap for animal to human efficacy data. *Animals (Basel)*. 2020;10(7).
6 Su Y, Chen D, Yuan D, et al. Multi-omics resolves a sharp disease-state shift between mild and moderate COVID-19. *Cell*. 2020;183(6):1479–1495.e20.
7 Schulte-Schrepping J, Reusch N, Paclik D, et al. Severe COVID-19 is marked by a dysregulated myeloid cell compartment. *Cell*. 2020;182(6):1419–1440.e23.
8 Sinha S, Rosin NL, Arora R, et al. Dexamethasone modulates immature neutrophils and interferon programming in severe COVID-19. *Nat Med*. 2022;28(1):201–211.
9 Bernardes JP, Mishra N, Tran F, et al. Longitudinal multi-omics analyses identify responses of megakaryocytes, erythroid cells, and plasmablasts as hallmarks of severe COVID-19. *Immunity*. 2020;53(6):1296–12314.e9.
10 Silvin A, Chapuis N, Dunsmore G, et al. Elevated calprotectin and abnormal myeloid cell subsets discriminate severe from mild COVID-19. *Cell*. 2020;182(6):1401–1418.e18.
11 Patel NG, Bhasin A, Feinglass JM, Angarone MP, Cohen ER, Barsuk JH. Mortality, critical illness, and mechanical ventilation among hospitalized patients with COVID-19 on therapeutic anticoagulants. *Thrombosis Update*. 2021;2:100027.
12 Fan C, Wu Y, Rui X, et al. Animal models for COVID-19: advances, gaps and perspectives. *Signal Transduct Target Ther*. 2022;7(1):220.
13 Ragan IK, Hartson LM, Dutt TS, et al. A whole virion vaccine for COVID-19 produced via a novel inactivation method and preliminary demonstration of efficacy in an animal challenge model. *Vaccines (Basel)*. 2021;9(4).
14 Lee JS, Koh JY, Yi K, et al. Single-cell transcriptome of bronchoalveolar lavage fluid reveals sequential change of macrophages during SARS-CoV-2 infection in ferrets. *Nat Commun*. 2021;12(1):4567.
15 Speranza E, Williamson BN, Feldmann F, et al. Single-cell RNA sequencing reveals SARS-CoV-2 infection dynamics in lungs of African green monkeys. *Sci Transl Med*. 2021;13(578).
16 Qin Z, Liu F, Blair R, et al. Endothelial cell infection and dysfunction, immune activation in severe COVID-19. *Theranostics*. 2021;11(16):8076–8091.
17 Imai M, Iwatsuki-Horimoto K, Hatta M, et al. Syrian hamsters as a small animal model for SARS-CoV-2 infection and countermeasure development. *Proc Natl Acad Sci U S A*. 2020;117(28):16587–16595.
18 Trimpert J, Vladimirova D, Dietert K, et al. The Roborovski dwarf hamster is A highly susceptible model for a rapid and fatal course of SARS-CoV-2 infection. *Cell Rep*. 2020;33(10):108488.
19 Gruber AD, Firsching TC, Trimpert J, Dietert K. Hamster models of COVID-19 pneumonia reviewed: how human can they be? *Vet Pathol*. 2022;59(4):528–545.
20 Li H, Ma Q, Ren J, et al. Immune responses of different COVID-19 vaccination strategies by analyzing single-cell RNA sequencing data from multiple tissues using machine learning methods. *Front Genet*. 2023;14:1157305.
21 Luecken MD, Buttner M, Chaichoompu K, et al. Benchmarking atlas-level data integration in single-cell genomics. *Nat Methods*. 2022;19(1):41–50.
22 Sikkema L, Ramirez-Suastegui C, Strobl DC, et al. An integrated cell atlas of the lung in health and disease. *Nat Med*. 2023;29(6):1563–1577.
23 Xu C, Lopez R, Mehlman E, Regier J, Jordan MI, Yosef N. Probabilistic harmonization and annotation of single-cell transcriptomics data with deep generative models. *Mol Syst Biol*. 2021;17(1):e9620.
24 Hrovatin K, Moinfar AA, Zappia L, et al. Integrating single-cell RNA-seq datasets with substantial batch effects. *bioRxiv*. 2024. https://doi.org/10.1101/2023.11.03.565463.
25 Kingma DP, Welling M. Auto-encoding variational bayes. *arXiv*. 2013. https://doi.org/10.48550/arXiv.1312.6114.
26 Kingma DP, Welling M. An introduction to variational autoencoders. *Found Trends Mach Learn*. 2019;12(4):307–392.
27 Gronbech CH, Vording MF, Timshel PN, Sonderby CK, Pers TH, Winther O. scVAE: variational auto-encoders for single-cell gene expression data. *Bioinformatics*. 2020;36(16):4415–4422.
28 De Donno C, Hediyeh-Zadeh S, Moinfar AA, et al. Population-level integration of single-cell datasets enables multi-scale analysis across samples. *Nat Methods*. 2023;20(11):1683–1692.
29 Lotfollahi M, Wolf FA, Theis FJ. scGen predicts single-cell perturbation responses. *Nat Methods*. 2019;16(8):715–721.
30 Heydari AA, Davalos OA, Zhao L, Hoyer KK, Sindi SS. ACTIVA: realistic single-cell RNA-seq generation with automatic cell-type identification using introspective variational autoencoders. *Bioinformatics*. 2022;38(8):2194–2201.
31 Lotfollahi M, Naghipourfar M, Theis FJ, Wolf FA. Conditional out-of-distribution generation for unpaired data using transfer VAE. *Bioinformatics*. 2020;36(Suppl_2):i610–i617.
32 Lotfollahi M, Naghipourfar M, Luecken MD, et al. Mapping single-cell data to reference atlases by transfer learning. *Nat Biotechnol*. 2022;40(1):121–130.
33 Tasaki S, Xu J, Avey DR, et al. Inferring protein expression changes from mRNA in Alzheimer's dementia using deep neural networks. *Nat Commun*. 2022;13(1):655.
34 Kana O, Nault R, Filipovic D, Marri D, Zacharewski T, Bhattacharya S. Generative modeling of single-cell gene expression for dose-dependent chemical perturbations. *Patterns (N Y)*. 2023;4(8):100817.
35 Nouailles G, Wyler E, Pennitz P, et al. Temporal omics analysis in Syrian hamsters unravel cellular effector responses to moderate COVID-19. *Nat Commun*. 2021;12(1):4869.
36 Osterrieder N, Bertzbach LD, Dietert K, et al. Age-dependent progression of SARS-CoV-2 infection in Syrian hamsters. *Viruses*. 2020;12(7).
37 Peidli S, Nouailles G, Wyler E, et al. Single-cell-resolved interspecies comparison shows a shared inflammatory axis and a dominant neutrophil-endothelial program in severe COVID-19. *Cell Rep*. 2024;43(6):114328.
38 Trimpert J, Dietert K, Firsching TC, et al. Development of safe and highly protective live-attenuated SARS-CoV-2 vaccine candidates by genome recoding. *Cell Rep*. 2021;36(5):109493.
39 Trimpert J, Adler JM, Eschke K, et al. Live attenuated virus vaccine protects against SARS-CoV-2 variants of concern B.1.1.7 (Alpha) and B.1.351 (Beta). *Sci Adv*. 2021;7(49):eabk0172.
40 Adler JM, Martin Vidal R, Voss A, et al. A non-transmissible live attenuated SARS-CoV-2 vaccine. *Mol Ther*. 2023;31(8):2391–2407.

41 Nouailles G, Adler JM, Pennitz P, et al. Live-attenuated vaccine sCPD9 elicits superior mucosal and systemic immunity to SARS-CoV-2 variants in hamsters. *Nat Microbiol*. 2023;8(5):860–874.
42 Haghverdi L, Buttner M, Wolf FA, Buettner F, Theis FJ. Diffusion pseudotime robustly reconstructs lineage branching. *Nat Methods*. 2016;13(10):845–848.
43 Law CW, Chen Y, Shi W, Smyth GK. voom: precision weights unlock linear model analysis tools for RNA-seq read counts. *Genome Biol*. 2014;15(2):R29.
44 Lun ATL, Richard AC, Marioni JC. Testing for differential abundance in mass cytometry data. *Nat Methods*. 2017;14(7):707–709.
45 Pennitz P, Kirsten H, Friedrich VD, et al. A pulmonologist's guide to perform and analyse cross-species single lung cell transcriptomics. *Eur Respir Rev*. 2022;31(165).
46 Hao Y, Stuart T, Kowalski MH, et al. Dictionary learning for integrative, multimodal and scalable single-cell analysis. *Nat Biotechnol*. 2023.
47 Dimitrov D, Turei D, Garrido-Rodriguez M, et al. Comparison of methods and resources for cell-cell communication inference from single-cell RNA-Seq data. *Nat Commun*. 2022;13(1):3224.
48 Turei D, Valdeolivas A, Gul L, et al. Integrated intra- and intercellular signaling knowledge for multicellular omics analysis. *Mol Syst Biol*. 2021;17(3):e9923.
49 Levy Y, Wiedemann A, Hejblum BP, et al. CD177, a specific marker of neutrophil activation, is associated with coronavirus disease 2019 severity and death. *iScience*. 2021;24(7):102711.
50 Aschenbrenner AC, Mouktaroudi M, Kramer B, et al. Disease severity-specific neutrophil signatures in blood transcriptomes stratify COVID-19 patients. *Genome Med*. 2021;13(1):7.
51 Seyhan AA. Lost in translation: the valley of death across preclinical and clinical divide—identification of problems and overcoming obstacles. *Transl Med Commun*. 2019;4(1):18.
52 Song Y, Miao Z, Brazma A, Papatheodorou I. Benchmarking strategies for cross-species integration of single-cell RNA sequencing data. *Nat Commun*. 2023;14(1):6495.
53 Maher AK, Burnham KL, Jones EM, et al. Transcriptional reprogramming from innate immune functions to a pro-thrombotic signature by monocytes in COVID-19. *Nat Commun*. 2022;13(1):7947.
54 Rocha SM, Fagre AC, Latham AS, et al. A novel glucocorticoid and androgen receptor modulator reduces viral entry and innate immune inflammatory responses in the Syrian hamster model of SARS-CoV-2 infection. *Front Immunol*. 2022;13:811430.
55 Abdelnabi R, Foo CS, Jochmans D, et al. The oral protease inhibitor (PF-07321332) protects Syrian hamsters against infection with SARS-CoV-2 variants of concern. *Nat Commun*. 2022;13(1):719.
56 Maio N, Cherry S, Schultz DC, Hurst BL, Linehan WM, Rouault TA. TEMPOL inhibits SARS-CoV-2 replication and development of lung disease in the Syrian hamster model. *iScience*. 2022;25(10):105074.
57 Lieber CM, Cox RM, Sourimant J, et al. SARS-CoV-2 VOC type and biological sex affect molnupiravir efficacy in severe COVID-19 dwarf hamster model. *Nat Commun*. 2022;13(1):4416.
58 Georg P, Astaburuaga-Garcia R, Bonaguro L, et al. Complement activation induces excessive T cell cytotoxicity in severe COVID-19. *Cell*. 2022;185(3):493–512.e25.
59 Witkowski M, Tizian C, Ferreira-Gomes M, et al. Untimely TGFbeta responses in COVID-19 limit antiviral functions of NK cells. *Nature*. 2021;600(7888):295–301.
60 Richardson S, Hirsch JS, Narasimhan M, et al. Presenting Characteristics, Comorbidities, and outcomes among 5700 patients hospitalized with COVID-19 in the New York City Area. *JAMA*. 2020;323(20):2052–2059.
61 Benitez ID, de Batlle J, Torres G, et al. Prognostic implications of comorbidity patterns in critically ill COVID-19 patients: a multicenter, observational study. *Lancet Reg Health Eur*. 2022;18:100422.
62 Wyler E, Adler JM, Eschke K, et al. Key benefits of dexamethasone and antibody treatment in COVID-19 hamster models revealed by single-cell transcriptomics. *Mol Ther*. 2022;30(5):1952–1965.
63 Meehan GR, Herder V, Allan J, et al. Phenotyping the virulence of SARS-CoV-2 variants in hamsters by digital pathology and machine learning. *PLoS Pathog*. 2023;19(11):e1011589.
64 Chu WT, Castro MA, Reza S, et al. Novel machine-learning analysis of SARS-CoV-2 infection in a subclinical nonhuman primate model using radiomics and blood biomarkers. *Sci Rep*. 2023;13(1):19607.
65 Virshup I, Bredikhin D, Heumos L, et al. The scverse project provides a computational ecosystem for single-cell omics data analysis. *Nat Biotechnol*. 2023;41(5):604–606.
66 Chua RL, Lukassen S, Trump S, et al. COVID-19 severity correlates with airway epithelium-immune cell interactions identified by single-cell analysis. *Nat Biotechnol*. 2020;38(8):970–979.
67 Grant RA, Morales-Nebreda L, Markov NS, et al. Circuits between infected macrophages and T cells in SARS-CoV-2 pneumonia. *Nature*. 2021;590(7847):635–641.
68 Wagner DE, Klein AM. Lineage tracing meets single-cell omics: opportunities and challenges. *Nat Rev Genet*. 2020;21(7):410–427.